Evidence of Time-dependent Sverdrup Circulation in the South Pacific from the Seasat Scatterometer and Altimeter

ALBERTO M. MESTAS-NUÑEZ, DUDLEY B. CHELTON, AND ROLAND A. DESZOEKE

College of Oceanography, Oregon State University, Corvallis, Oregon

7 January 1991 and 17 October 1991

ABSTRACT

Seasat scatterometer and altimeter data are analyzed to investigate time-dependent Sverdrup dynamics in the Southern Ocean (40°S to 60°S) over seasonal time scales. Sverdrup dynamics are shown to be inadequate to describe the circulation in the South Atlantic and Indian oceans. The Sverdrup circulation in the South Pacific is reasonable north of 55°S. The changes in Sverdrup circulation from July to September 1978 indicate an eastward acceleration along 55°S and westward acceleration along 40°S, suggesting a southward shift in the subpolar eastward flow. Sea level in the South Pacific is estimated for July and September 1978 from scatterometer vector wind data based on Sverdrup dynamics assuming a flat-bottom ocean with barotropic flow. The changes in Sverdrup sea level are compared with the changes in sea level observed by the altimeter for the same time period. Both estimates indicate a rise in sea level along a zonal band centered at about 50°S. This sea level rise inferred from both the scatterometer and altimeter data is supported by a similar rise in sea level observed from tide gauge measurements at two locations in New Zealand. The spatial correlation between the two satellite estimates of sea level change is about 0.5. This agreement suggests that time-dependent Sverdrup dynamics may account for about 1/4 of the spatial variance of sea level change in the South Pacific over the 3-month Seasat mission.

1. Introduction

The simplest model of wind-forced ocean circulation is the classical Sverdrup model for the ocean interior (Sverdrup 1947). In the Sverdrup model, the vorticity input by the wind at the sea surface (given by the wind-stress curl) is balanced by the advection of planetary vorticity in the water column. Stommel (1957) suggested the possibility of a Sverdrup balance for the Antarctic Circumpolar Current (ACC) with the Scotia Island Arc 2000 km to the east of Drake Passage (Fig. 1) acting as an eastern boundary. Baker (1982) and Godfrey (1989) presented evidence supporting this hypothesis for the region at and north of 55°S. The quality of the wind fields used in these studies has been questioned, however, and Chelton et al. (1990a) were unable to demonstrate a Sverdrup balance at 55°S from 3 months of high quality scatterometer winds. In addition, the modeling study of Clarke (1982) suggests that the Sverdrup balance may not hold south of 55°S.

The validity of the Sverdrup balance for the mean flow in the ACC is thus not completely established. However, recent evidence suggests that Sverdrup dynamics may describe the variability of the ACC over seasonal time scales. Peterson (1988) argued that changes in wind-stress curl would produce changes in the meridional transport across the northern and southern boundaries of the ACC and therefore changes in the pressure field within the current, consistent with Sverdrup dynamics. His comparisons of time series of zonally averaged wind-stress curl along the boundaries of the ACC with bottom pressure records at a northern and a southern location in the Drake Passage are generally consistent with the required condition of pressure changes being inversely related to the curl in the north and directly related to it in the south.

In this paper, time-dependent Sverdrup dynamics in the Southern Ocean are investigated over a 3-month period using a barotropic model of the temporal variability of ocean circulation. The assumption of barotropic variability yields a very simple relation between sea level and wind stress. There is some justification from observations for modeling the variability as barotropic. Whitworth and Peterson (1985) have argued that the mean flow through Drake Passage is 70% baroclinic, but fluctuations about the mean are almost totally barotropic. The barotropic circulation is consid-

Corresponding author address: Dr. Dudley B. Chelton, Oregon State University, College of Oceanography, Corvallis, OR 97331.

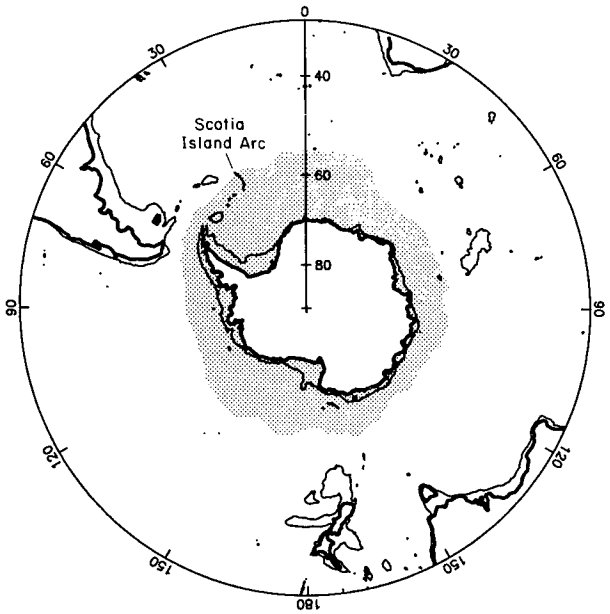

FIG. 1. Map of the Southern Ocean with the 1000-m bathymetry (thin lines) and maximum ice boundary (shaded region) for the Seasat period.

ered here to be in equilibrium with the monthly mean winds so that the interior ocean is governed by a time-dependent Sverdrup balance.

The wind and sea level data used in this study were measured simultaneously by the scatterometer and altimeter aboard the Seasat satellite, which operated from 7 July to 10 October 1978. The satellite data are described in section 2. The global Sverdrup circulation computed from the scatterometer data for the first and last months of the Seasat mission (July and September 1978) are presented and interpreted in section 3. In section 4, a simple model relating the Sverdrup transport streamfunction to sea level is introduced; the temporal changes in sea level in the South Pacific estimated from the scatterometer data are then compared with the changes observed by the altimeter. The implications of the results are discussed in section 5.

2. Data description

a. *Wind stress*

The Seasat-A Satellite Scatterometer (SASS) vector winds used here were produced by Atlas et al. (1987) (see also Chelton et al. 1989). The spatial resolution of these vector winds is about 100 km. The data were binned into 2° × 2° boxes for the three 1-month periods of "July," "August," and "September," defined to be 7 July–6 August, 7 August–6 September, and 7 September–10 October, respectively, to allow three complete months of data from the Seasat mission.

The SASS estimates of 19.5-m neutral-stability wind speed and direction were used to generate the vector average of the surface stress following the methodology of Chelton et al. (1990a). Briefly, the wind speed was first corrected for a 1 m s^{-1} bias known to exist in the Atlas et al. (1987) SASS data. The 19.5-m neutral-stability wind vectors were brought to a height of 10 m by a neutral-stability multiplicative scaling factor of 0.943. The surface wind stress τ was then computed for each SASS observation of 10-m winds using the bulk aerodynamic formula with the wind-speed–dependent drag coefficient of Large and Pond (1982). Observations south of a maximum ice boundary determined from passive microwave remote sensing (Fig. 1) were eliminated.

The raw 2° × 2° average τ fields showed zonally periodic structure symptomatic of sampling error from spatially inhomogeneous sampling in the monthly averages. The same bell-shaped low-pass filter used by Chelton et al. (1990a) was applied here to generate smoothed 2° × 2° fields analogous to 5° latitude by 16° longitude averages, though with a much better wavenumber transfer function than a simple running average.

b. *Wind-stress curl*

The wind-stress curl was computed in spherical polar coordinates to allow for the convergence of meridians at high latitudes (Neumann 1955). The expression for the radial component of the wind stress curl at each grid point is

$$(\nabla \times \tau)_r = \frac{1}{R\cos\theta}\left[-\frac{\partial(\tau_\phi \cos\theta)}{\partial\theta} + \frac{\partial\tau_\theta}{\partial\phi}\right], \quad (1)$$

where θ and ϕ are latitude and longitude, respectively, and R is the radius of the earth. The subscripts r, θ, and ϕ denote the radial, latitudinal, and longitudinal vector components. Except at the extreme northern and southern latitudes, the spatial derivatives were computed using quotients of centered finite first differences on the 2° × 2° grid; the meridional derivatives at the extreme latitudes were computed using uncentered differences. Elsewhere, derivatives were not computed if any of the required observations for centered differences were missing (i.e., observations near land or the maximum ice boundary).

c. *Sea level*

The sea level fields used in this study were produced by Fu and Chelton (1985). Each gridded time series of sea level (relative to an unknown reference level) was obtained from crossover sea-level differences between ascending and descending

satellite ground tracks near the grid point. The technique can be explained briefly by considering a small area A containing M ascending and N descending tracks. Estimation of the $M + N$ unknown along-track mean sea levels over A from the $M \times N$ crossover difference observations in A is an overdetermined problem. The solutions are determined by least squares, subject to the requirement that the solution for mean sea level along one of the tracks through A be specified to avoid a singular matrix. The time series of sea level is obtained by ordering the solutions by time and setting the value of mean sea level along the first track across the area A to zero.

Fu and Chelton (1985) performed the analysis for 229 areas in the Southern Ocean, each with approximate area $A \approx 200 \times 200$ km^2. The locations of the centers of the areas resemble a 4°latitude by 10°longitude irregular grid (see their Fig. 8). To increase the signal-to-noise ratio, each time series was smoothed with an effective 20-day running average. The sea level data analyzed here are thus representative of variability over spatial scales larger than 200 km and time scales longer than 20 days. For the analysis presented here, the Fu and Chelton (1985) gridded sea level fields were interpolated onto the regular $2° \times 2°$ grid by cubic spline interpolation and low-pass filtered in space to resolve the same scales as the wind stress described in section 2a.

3. Southern Hemisphere Sverdrup circulation

It can easily be shown (Sverdrup 1947) that the depth-integrated, linearized steady-state equations of motion of an inviscid flat-bottom ocean in spherical coordinates reduce to the Sverdrup balance

$$\frac{\beta}{R\cos\theta}\frac{\partial\psi}{\partial\phi} = \frac{(\nabla \times \tau)_r}{\rho_o}, \tag{2}$$

where ψ is the streamfunction of vertically integrated volume transport, ρ_o is a representative density of the water column, and $\beta = (2\Omega \cos\theta)/R$ is the meridional gradient of the Coriolis parameter $f = 2\Omega \sin\theta$ for earth rotation rate Ω.

The volume transport streamfunction ψ can be obtained by zonal integration of the Sverdrup equation (2) from an eastern boundary starting with a constant initial value ψ_o, imposed to satisfy the boundary condition of no normal flow. This constant is set to zero at Africa and South America, but not at Antarctica (to allow for Drake Passage throughflow) nor at Australia–New Guinea (considered as a single landmass) or New Zealand to allow circulation around "islands" as first suggested by Godfrey (see Godfrey 1989; deSzoeke 1987; and Chelton et al. 1990a). Using the nomenclature of deSzoeke (1987) and his Fig. 15 to define the closed integration paths, the streamfunction values ψ_o for New Zealand and Australia can be written as

$$\psi_{NZ} = \frac{1}{\rho_o(f_S - f_N)} \oint \tau \cdot d\mathbf{l} \tag{3a}$$

$$\psi_{AUS} = \frac{\oint \tau \cdot d\mathbf{l} - \rho_o(f_S - f_{TAS})\psi_{NZ}}{\rho_o(f_{TAS} - f_{NG})}, \tag{3b}$$

respectively, where f_{NG}, f_{TAS} are the values of the Coriolis parameter at the limiting northern (New Guinea) and southern (Tasmania) latitudes of Australia–New Guinea, and f_N, f_S are the same for New Zealand.

The latitude circles that pass through Drake Passage lack a well-defined eastern boundary. However, as first noted by Stommel (1957), the Scotia Island Arc imposes a severe restriction on the flow 2000 km downstream of Drake Passage because no latitude can cross it without encountering water depths shallower than 1000 m (see Fig. 1). Hence, in the present study, the integration of (2) at these latitudes is initiated at the Scotia Island Arc, which is considered as an extension of the Antarctic Peninsula. According to Whitworth and Peterson (1985), the mean transport through Drake Passage is 120 Sv (1 Sv $\equiv 10^6$ m^3 s^{-1}). Since ψ_o is zero along the boundary of South America, the corresponding mean value of ψ_{ANT} on the Antarctic continent (including the Scotia Island Arc) must be 120 Sv. For the analysis presented here, we allow ψ_{ANT} to increase from 110 Sv for July 1978 to 130 Sv for September 1978, consistent with Whitworth and Peterson's (1985) 20-Sv seasonal increase in the transport through Drake Passage (see their Fig. 7). Imposing this seasonal change in transport does not alter the conclusions of this study.

The global Sverdrup circulation north of 55°S forced by the 96-day average Seasat winds has previously been presented by Chelton et al. (1990a). Here we attempt to include the latitude band between 55°S and 60°S as discussed above and examine the changes in Southern Hemisphere subtropical Sverdrup circulation from the beginning to the end of the Seasat mission. The streamfunctions ψ for July and September computed by integrating (2) and the differences (September minus July), which are proportional to the accelerations of the Sverdrup flow, are shown in Fig. 2.

Since (2) is strictly valid only for steady-state motions, some discussion of the concept of time-dependent Sverdrup dynamics is necessary. Over the short time scales resolvable by the 3-month Seasat dataset, only the barotropic circulation can come into equilibrium with the wind forcing. The spinup time of the depth-integrated barotropic circulation is given by the time required for

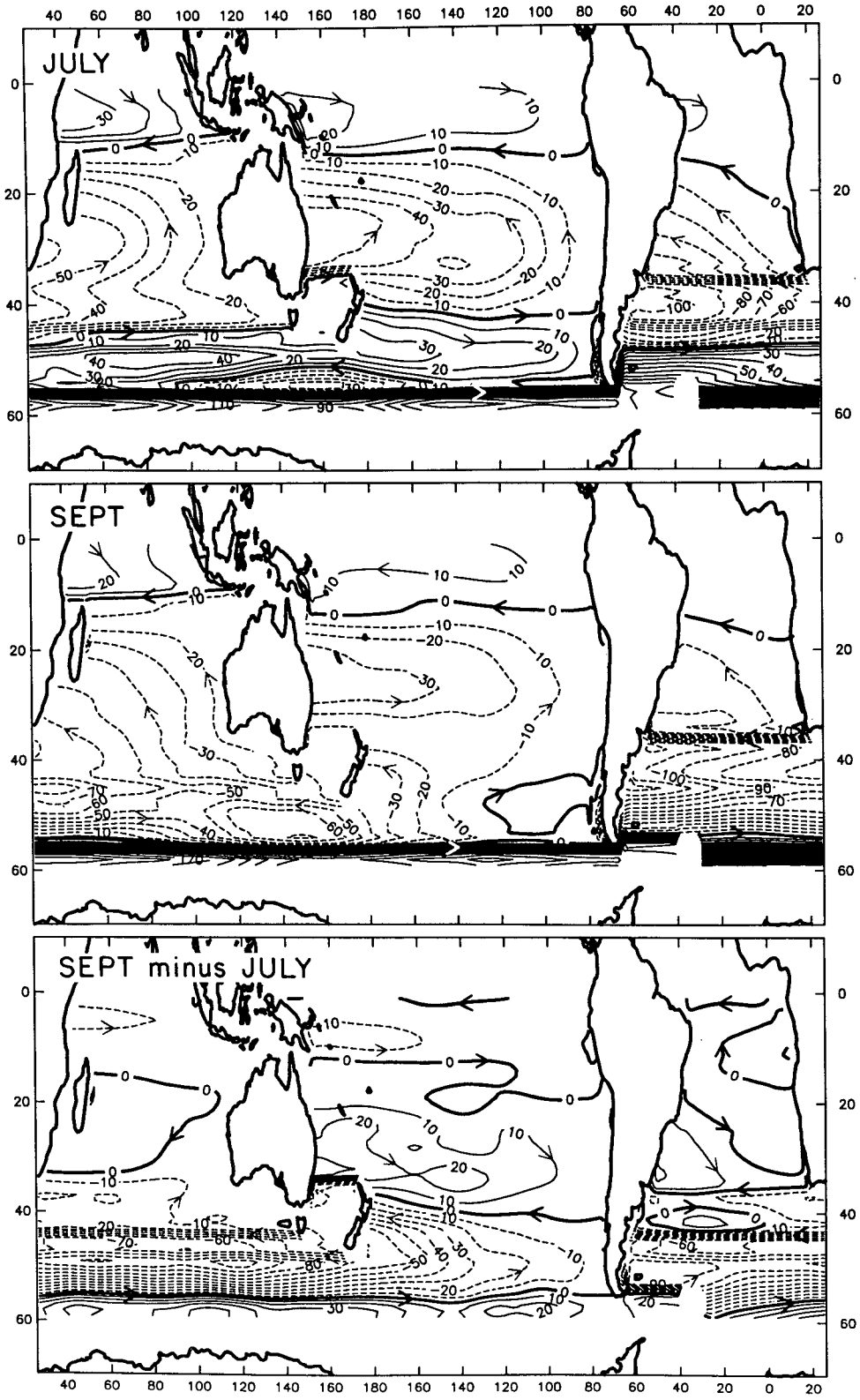

FIG. 2. Sverdrup transport streamfunction in 10^6 m^3 s^{-1} (Sv) computed from the SASS winds for July 1978 (upper) and September 1978 (middle). The change in Sverdrup circulation (September minus July) is shown in the lower panel.

barotropic Rossby waves to cross the basin. The time-dependent barotropic response to wind stress is given by

$$\frac{\partial}{\partial t}\nabla^2\psi_{bt} + \frac{\beta}{R\cos\theta}\frac{\partial\psi_{bt}}{\partial\theta} = \frac{(\nabla\times\tau)_\tau}{\rho_o}. \quad (4)$$

(The effects of advection and diffusion of vorticity, variation of bottom topography, and bottom drag have been neglected.) Neglect of the unsteady term gives a barotropic version of the Sverdrup equation (2). At the basin scales of forcing disturbances evident in Fig. 2, the relative vorticity is approximately $\nabla^2\psi_{bt} \approx -L^{-2}\psi_{bt}$, where $L \gtrsim$ O(1000 km). This makes (4) resemble a simple one-dimensional wave equation with a westward phase speed of order $\beta L^2 \approx 18$ m s^{-1} at 40°S. For a basin width of 1.2×10^4 km in the South Pacific, the corresponding adjustment time is about 8 days. On longer time scales, say months, the quasi-steady response embodied in (2) ought to be well established.

For latitudes south of Australia and New Zealand, the basin width is more than twice as large (the circumpolar span of the ACC). The circulation adjustment of the full Southern Ocean is therefore more than two weeks, and an equilibrium adjustment to monthly mean winds at high southern latitudes is more difficult to rationalize. The computed Sverdrup circulations are nonetheless indicative of the tendency of the ocean to respond to temporal changes in wind forcing. The degree of accuracy of the resulting circulation patterns for each month depends on the relative importances of barotropic versus baroclinic flow, as well as on the validity of the Sverdrup dynamics.

Several shortcomings of the simple Sverdrup model are immediately apparent. The most outstanding is the discontinuity in streamfunction emanating from the southern tip of South America and the northern tip of the Antarctic Peninsula/Scotia Island Arc at 55°S and associated with the 120-Sv transport across Drake Passage. This discontinuity is purely zonal with no meridional migration as it girdles the pole (although its strength varies somewhat as streamlines leave or join it) and is the model's crude representation of the core of the ACC. Similar zonal jet discontinuities extend westward from the southern boundaries of all landmasses in the Southern Hemisphere (Africa, Tasmania, and New Zealand) and westward from the northern boundaries of New Zealand and Australia. These zonal jets are present in both July and September but are especially pronounced in July when they are augmented by a divergent Sverdrup circulation in the South Pacific along 40°S [Fig. 3; see also Fig. 5 of Chelton et al. (1990a)].

These jetlike discontinuities could have been ameliorated in the model by including frictional mechanisms to smear the cores across internal zonal boundary layers (Gill 1968), just as friction can be invoked to close the Sverdrup circulation on western boundaries of ocean basins. Indeed, the zonal jets in the model exist to lead off the surplus or bring in the deficit water transport in the western boundary currents on the continents and islands where the landmasses abruptly end. Along latitudes interrupted by a landmass, the zonal integration of (2) must be stopped at the eastern boundary of the landmass and restarted at the western boundary with a new value of the streamfunction, imposed as zero for South America and Africa, computed by the island rule (3) for Australia and New Zealand, or imposed as the transport through Drake Passage for the Antarctic Peninsula/Scotia Island Arc. The difference between the streamfunction value along the boundary of the landmass and the value just east of the landmass computed from (2) defines the transport of the western boundary current at that location.

At the latitudinal extremities of Australia and New Zealand, the western boundary currents need not vanish. The boundary currents must therefore feed or be supplied by zonal jets extending westward from those extremities. The jets do not waver because they must follow constant latitude lines in the flat-bottom Sverdrup model. It has been remarked that the zonal meandering of the core of the ACC is associated with bottom topography (Gordon et al. 1978; Chelton et al. 1990b). Given the lack of topography in the simple Sverdrup model, it is not surprising that the model jets cannot reproduce this meandering. Such zonal jets do not appear in maps of Northern Hemisphere Sverdrup circulation because there are no significant unconnected landmasses to interrupt the zonal integration of the Sverdrup equation (2). Because of these shortcomings, the Sverdrup circulations are not realistic in the South Atlantic and south Indian and throughout the Southern Ocean south of 55°S where the zonal jets are most pronounced.

Stommel's (1957) suggestion for estimating Sverdrup circulation in the Southern Ocean evidently does not produce quantitatively accurate circulation patterns south of 55°S. In general, then, a suitable model of the circulation must include higher-order dynamics such as eddy fluxes and topographic pressure drag (e.g., Johnson and Bryden 1989). The only region where the Sverdrup circulation in Fig. 2 appears reasonable is the South Pacific, equatorward of 55°S, a region where the Sverdrup balance has previously been shown to provide a good description of the mean circulation (deSzoeke 1987). In the remainder of this paper,

attention is therefore restricted to the subtropical circulation in the South Pacific.

The dramatic changes from July to September in the South Pacific merit special attention. The model net meridional transport between South America and New Zealand is given simply by $-\psi_{NZ}$, which is the sum of the interior Sverdrup transport plus the western boundary current transport along the east coast of New Zealand. Between July and September 1978, this model meridional transport changed from 8 Sv southward to 25 Sv northward. Since ψ_{AUS} remained nearly constant (16 Sv in July and 17 Sv in September), most of this 33-Sv northward increase was compensated by a 32-Sv southward increase in the model meridional transport within the Tasman Sea; the net meridional transport in the Tasman Sea (given by the difference $\psi_{NZ} - \psi_{AUS}$) changed from 24 Sv northward in July to 8 Sv southward in September. The 1-Sv change in meridional transport in the total South Pacific (South America to Australia) from July to September was balanced by a 1-Sv increase in the Indonesian throughflow from the Pacific to the Indian Ocean.

The mass balance between the Tasman Sea and the interior South Pacific was achieved by the zonal jets west of the extreme latitudes of New Zealand discussed above. The zonal flow along the northern latitude of New Zealand [approximately coincident with the Tasman Front—see Stanton (1981); Mulhearn (1987)] changed from 33 Sv eastward in July to 12 Sv westward in September. At the same time, the zonal flow west of the southern latitude of New Zealand changed from 25 Sv eastward to 12 Sv westward.

The extreme changes in Sverdrup circulation within the Tasman Sea are remarkable. It should be emphasized that these "circulations" are the equilibrium circulations that would be achieved eventually if the model ocean were allowed to adjust to the winds of the respective months. The largest factor in the changes is the dramatic variation of ψ_{NZ} computed from the island rule (3) between July and September. These changes in the equilibrium Sverdrup circulation are indicative of very large changes in the wind forcing over the South Pacific during the 3-month period of the Seasat mission. The feature in the meteorological fields responsible for the July circulation pattern was an anomalous blocking high southeast of New Zealand accompanied by a strong cutoff low to the northeast (Chelton et al. 1990a); the Sverdrup circulation computed from the July 1978 winds is therefore not representative of the long-term average July circulation. Indeed, the July 1978 circulation of the South Pacific is difficult to reconcile with the traditional view of the surface circulation inferred from hydrographic data (Gordon et al. 1978). In particular, the Sverdrup flow near 55°S was everywhere westward in the South Pacific, counter to the mean ACC.

The westward Sverdrup transport at high southern latitudes is not unique to the scatterometer dataset. We have computed similar westward transports from surface wind analyses produced by the European Centre for Medium Range Weather Forecasts (ECMWF) (not shown here). While such westward Sverdrup transport deviates from conventional wisdom, Godfrey (1989) and Chelton et al. (1990a) have pointed out that the depth-integrated flow inferred from hydrographic data is westward south of Australia and New Zealand (Wyrtki 1971; Reid 1986). It must be kept in mind that the temporal variability of the vertically integrated transport at these latitudes is not presently well known. This is especially true during the Southern Hemisphere winter season of the Seasat mission and during anomalous meteorological conditions such as experienced in the South Pacific during July 1978.

It is noteworthy that an apparent westward surface flow extending from the southeast to the central South Pacific between 40°S and 45°S has previously been suggested by Deacon (1977) based on climatological, as well as single-season (May–July 1968), water mass characteristics. The possibility of westward vertically integrated transport at high latitudes in the South Pacific during July 1978 therefore cannot be categorically rejected. In contrast to July 1978, the meteorological conditions were nearly normal during September 1978 (Chelton et al. 1990a). The resulting Sverdrup circulation was eastward at the highest latitudes (near 55°S) with broad equatorward flow over most of the interior basin, turning westward north of about 25°S. This circulation pattern is consistent with the circulation inferred from hydrographic data.

Despite the limitations of the time-dependent Sverdrup model, it can be argued that the circulation computed from models with more sophisticated dynamics would probably also yield a significant response to the large changes in wind forcing between July and September. The change in Sverdrup circulation in the lower panel of Fig. 2 can therefore be considered as the tendency for change in the barotropic circulation from July to September 1978. The flow pattern in the interior South Pacific indicates opposing zonal acceleration north and south of approximately 50°S, with eastward acceleration on the south side and westward acceleration on the north side. This can be interpreted as a southward shift of the subpolar eastward flow in the South Pacific. Indeed, while the maximum of the trade winds in the South Pacific maintained its position (15°S) and strength from July to September 1978, the

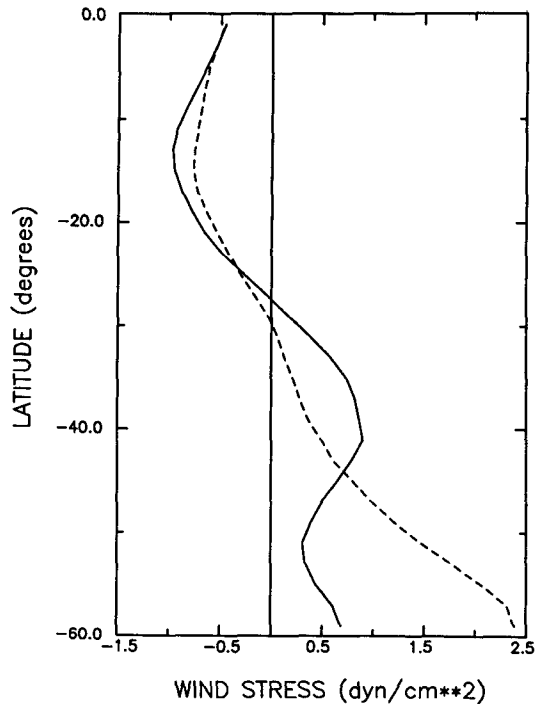

FIG. 3. Latitudinal profiles of zonally averaged eastward component of SASS wind stress in the South Pacific for July (solid line) and September (dashed line).

maximum of the westerlies shifted southward from 40°S to 60°S and increased in amplitude by a factor of two (Fig. 3).

4. Sea level changes in the South Pacific

The validity of the changes in Sverdrup circulation in Fig. 2 inferred from the scatterometer data can be investigated by comparison with changes in the geostrophic surface circulation inferred from Seasat altimeter data. As noted previously, only the barotropic component can adjust quickly enough to reach equilibrium over the full South Pacific over the seasonal time scales resolvable by the 3-month Seasat dataset. A barotropic Sverdrup model therefore seems appropriate as a first-order model of the circulation over short time scales.

Since the motion is geostrophic, the relationship between sea level change over 3 months to the change in barotropic streamfunction is

$$\Delta\eta = \frac{f}{gH}\Delta\psi_{bt}, \tag{5}$$

where H is mean water depth, which we take to be 4 km. Hence (2) becomes

$$\frac{\beta gH}{fR\cos\theta}\frac{\partial\Delta\eta}{\partial\phi} = \Delta\left[\frac{(\nabla\times\tau)_r}{\rho_o}\right], \tag{6}$$

where the right-hand side is the change in wind-stress curl over the 3 months.

The Sverdrup sea level changes in the South Pacific were computed by zonally integrating (6) for comparison with the altimeter data. Since the sea level change from July to September 1978 in the barotropic model is equal to the change in Sverdrup streamfunction scaled by the factor f/gH, the pattern of sea level change (Fig. 4) is very similar to the change in Sverdrup circulation in the South Pacific (Fig. 2, lower panel). The two patterns are opposite in sign because $f < 0$.

The field of sea level change from the altimeter is shown in Fig. 5. The Sverdrup and altimeter estimates of sea level change both indicate a ridge of sea level rise in the western South Pacific along approximately 50°S, with nodal lines along approximately 40°S and 55°S. A scatterplot comparison of the two gridded fields of sea level change is shown in Fig. 6. The two outlier points (circled) come from the region east of the East Pacific Rise, where the altimeter observed sea level decreases of more than 10 cm that the Sverdrup model did not reproduce. This disagreement might be attributable to neglect of topographic effects in the model.

The spatial correlation between Sverdrup and altimeter estimates of sea level change is 0.54. Using a bootstrap technique (Effron 1979), we estimate the ±1 standard deviation uncertainty of this correlation to be ±0.09. Since the 95% confidence interval on the sample correlation is approximately twice the standard deviation, the sample correlation is statistically significant with greater than 95% confidence. The regression coefficient between $\Delta\eta_{alt}$ and $\Delta\eta_{Sv}$ from Fig. 6 is 0.3, indicating that the observed sea level change is only about 1/3 of that predicted by the Sverdrup model. The possibility of mechanisms other than Sverdrup dynamics playing a relevant role cannot be ruled out.

The altimeter and Sverdrup sea level changes for the July–August period (not shown) are qualitatively consistent with the July–September results presented in this section. However, the dynamic range of the July–August sea level change is rather small, and further quantitative comparisons become impractical.

5. Summary and discussion

We have calculated the Southern Hemisphere Sverdrup circulation from spatially smoothed monthly average Seasat scatterometer estimates of wind stress during July and September 1978. These quasi-equilibrium monthly Sverdrup circulations ought to represent the large-scale barotropic response to changes in wind forcing.

In contrast to the Northern Hemisphere, calculation of the Sverdrup circulation in the Southern

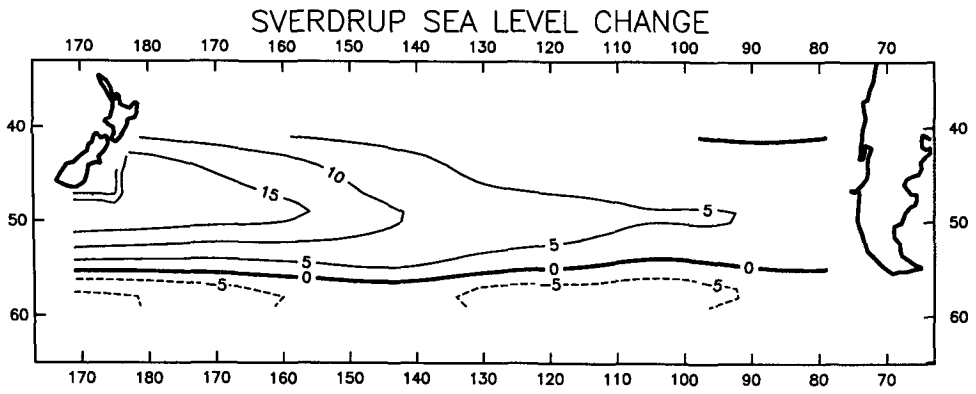

FIG. 4. Map of Sverdrup sea level changes in centimeters over the South Pacific (September minus July).

Hemisphere is complicated by the presence of "islands" (New Zealand and Australia) that interrupt the zonal integration of the wind-stress curl and by the fact that there is no meridional landmass barrier at which to begin the zonal integration between 55°S (the southern tip of South America) and 65°S (the northern tip of the Antarctic Peninsula). These problems were dealt with here by using the "island rule" to determine the streamfunction values along the coasts of New Zealand and Australia and by considering the Scotia Island Arc as an extension of the Antarctic Peninsula and specifying the streamfunction around Antarctica to give the observed Drake Passage mass transport.

A remarkable feature of the July–September change in the Seasat scatterometer winds is the large change in the value of ψ_{NZ} by the island rule, from 8 Sv to −25 Sv. Independent evidence for such a change may be cited from New Zealand tide gauge data. The monthly mean sea levels at Waitemata (36.8°S, 174.8°E) and Wellington (41.3°S, 174.8°E), corrected for a 1 cm/mb inverse barometer effect, rose by 10 cm and 9 cm, respectively, from July to September. This is of the same order as the 8-cm barotropic Sverdrup sea level change computed from (5).

The island rule leads to the shedding of zonal jet discontinuities west of the latitudinal extremities of New Zealand, Australia, Africa, and South America. These discontinuities, which might have been moderated by the inclusion in the model of higher-order effects such as friction, dominate the charts of Fig. 2, except in the South Pacific north of 55°S. For this reason, we have focused attention on the Sverdrup circulation in the subantarctic/subtropical sector of the South Pacific.

Over the 3-month period of the Seasat mission, only the barotropic circulation can equilibrate with the wind forcing. A barotropic model of the Sverdrup circulation furnishes a simple relation between the wind-generated streamfunction and sea level. The resulting change in Sverdrup sea level in the South Pacific from July to September 1978 compares favorably with the spatially smoothed sea level change measured by the altimeter. Both patterns of sea level change consist of a zonal band of sea level rise along approximately 50°S with a larger amplitude in the western part of the basin. Both estimates of sea level also show nodal lines along approximately 40°S and 55°S.

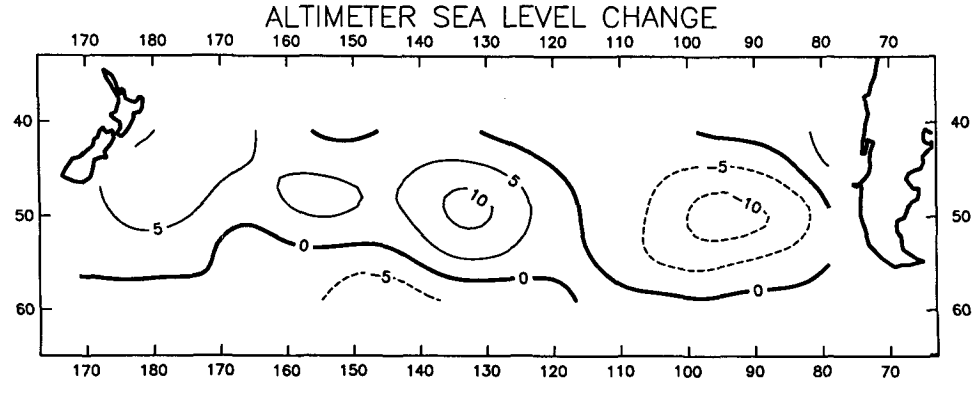

FIG. 5. Map of altimeter sea level changes in centimeters over the South Pacific (September minus July).

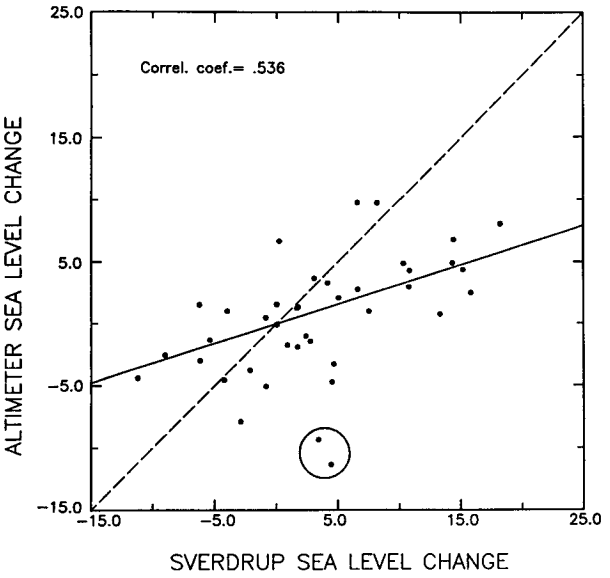

FIG. 6. Scatterplot comparison of Sverdrup and altimeter sea level changes (both in cm) in a 4°by 14°grid for the South Pacific. The regression line through the origin (solid line) has slope 0.3.

The calculated and observed sea level change over the 3-month Seasat mission can be interpreted as a southward shift of the subtropical front. A very similar change in the circulation has been inferred by Large and van Loon (1989) from analysis of the drift velocities of FGGE buoys during 1979. They argue that the zonal bands of eastward and westward acceleration are a seasonal barotropic response to a semiannual latitudinal shift in the westerly winds of the Southern Hemisphere. The zonal bands of acceleration in the South Pacific inferred here from 3 months of Southern Hemisphere winter Seasat scatterometer and altimeter data have also been observed during two consecutive Southern Hemisphere winters from Geosat altimeter data (Chelton et al. 1990b). The Geosat data support the interpretation of this pattern of variability as being part of a semiannual signal as suggested by Large and van Loon (1989).

The effects of bottom topography have been neglected in the simple model considered here. For seasonal changes at midlatitudes, the relation that is believed to hold is the topographic Sverdrup balance (Gill and Niiler 1973; Willebrand et al. 1980). However, Koblinsky et al. (1989) found that the topographic Sverdrup equation could explain the variability of deep ocean currents only at localized regions in the North Pacific. The validity of the topographic Sverdrup balance at those locations has also been questioned by recent numerical experiments (Cummings 1991). Greatbatch and Goulding (1989) showed that away from the western boundary currents, the barotropic seasonal changes of the North Pacific circulation are well represented by a flat-bottom model. They considered this result to be related to the simple zonal structure of the f/H contours in that basin. In the South Pacific this argument cannot be made since the f/H contours are more complicated. In the southeastern Pacific, for example, f/H contours are closed [see Plate 1 of Koblinsky (1990)].

We have investigated the extreme case of the topographic Sverdrup model in the South Pacific. The resulting acceleration bands follow f/H contours. In the southwestern South Pacific, the f/H contours are nearly zonal but the zonal acceleration bands were opposite in direction to the zonal bands inferred from the flat-bottom Sverdrup model, which contradicts the altimetric observations. In addition, in the southeastern South Pacific where the f/H contours are closed, the topographic Sverdrup model becomes inappropriate. We have therefore presented only the results for the flat-bottom case.

Anderson and Killworth (1977) [see also Anderson et al. (1979)] studied the spinup of a two-layer ocean with topography and showed that the topography induces interaction between the dynamic modes. As a result of this interaction, the barotropic adjustment occurs on two time scales. First, there is a rapid adjustment (days) to a topographic Sverdrup balance. On a slower time scale (years), the baroclinic mode smooths out the effects of bottom topography and forces the barotropic mode more toward a flat-bottom Sverdrup balance. For an intermediate stage of incomplete baroclinic adjustment, such as for a time scale of several months, the barotropic response dominates and the effects of the baroclinic adjustment are difficult to quantify.

In the present study, we have neglected baroclinic effects based on arguments presented by Whitworth and Peterson (1985) from analysis of pressure gauge observations at Drake Passage. However, it has been argued that pressure gauges could effectively filter out baroclinic motions (Willebrand et al. 1980). Indeed, a vertical modal decomposition of current meter observations (using empirical orthogonal functions) shows that the low-frequency variability at Drake Passage is surface intensified and can be interpreted as a superposition of barotropic and first baroclinic modes (Inoue 1985), suggesting that coupling between the dynamic modes cannot be neglected. The success of the flat-bottom barotropic Sverdrup model in explaining the altimeter sea level patterns could be coincidental. An alternative explanation is that, even on seasonal time scales, the coupling between the first two dynamic modes (as suggested by Inoue) is important and could smooth out the topographic effects on the barotropic mode.

In conclusion, although the statistical signifi-

cance of the results presented here is rather limited by the short 3-month duration of the Seasat mission, the analysis is suggestive of a Sverdrup-like response of the large-scale circulation of the South Pacific to changes in wind forcing. The discrepancy between modeled and observed sea level response indicates that time-dependent Sverdrup dynamics may not be the only important mechanism. The nature of this response appears to be a seasonal signal associated with large seasonal changes in the wind forcing. At present, there are other wind products such as the ECMWF surface wind analyses (e.g., Trenberth et al. 1990) that may be appropriate for investigating this question, although the quality of these analyses at high latitudes in the Southern Hemisphere is still uncertain. Based on the analysis presented in this paper, the South Pacific is a promising region to investigate large-scale response to time-variable wind forcing from a more sophisticated model than the simple Sverdrup model considered here.

Acknowledgments. We thank Robert Atlas for providing the SASS vector wind data and Gary Mitchum for providing the New Zealand tide gauge data used in this investigation. We also thank Ayal Anis, Michael Freilich, Ricardo Matano, Jim Richman, and Donna Witter for helpful discussions and comments on an early draft of this manuscript. The research described in this paper was supported by Contract 957580 from the Jet Propulsion Laboratory funded under the NSCAT Announcement of Opportunity and by NASA Grant NAGW-730.

REFERENCES

Anderson, D. L., and P. D. Killworth, 1977: Spin-up of a stratified ocean, with topography. *Deep-Sea Res.*, **24,** 709–732.

——, K. Bryan, A. E. Gill, and R.C. Pacanowski, 1979: The transient response of the North Atlantic: Some model studies. *J. Geophys. Res.*, **84,** 4795–4815.

Atlas, R., A. J. Busalacchi, M. Ghil, S. Bloom, and E. Kalnay, 1987: Global surface wind and flux fields from model assimilation of Seasat data. *J. Geophys. Res.*, **92,** 6477–6487.

Baker, D. J., Jr., 1982: A note on Sverdrup balance in the Southern Ocean. *J. Mar. Res.*, **40** (Suppl.), 21–26.

Chelton, D. B., M. H. Freilich, and J. R. Johnson, 1989: Evaluation of unambiguous vector winds from the Seasat scatterometer. *J. Atmos. Oceanic Technol.*, **6,** 1024–1039.

——, A. M. Mestas-Nuñez, and M. H. Freilich, 1990a: Global wind stress, wind stress curl, and Sverdrup circulation from the Seasat scatterometer. *J. Phys. Oceanogr.*, **20,** 1175–1205.

——, M. G. Schlax, D. L. Witter, and J. G. Richman, 1990b: Geosat altimeter observations of the surface circulation of the Southern Ocean. *J. Geophys. Res.*, **95,** 17 877–17 903.

Clarke, A. J., 1982: The dynamics of large-scale, wind-driven variations in the Antarctic Circumpolar Current. *J. Phys. Oceanogr.*, **12,** 1092–1105.

Cummings, P. F., 1991: The barotropic response of the subpolar North Pacific to stochastic wind forcing. *J. Geophys. Res.*, **96,** 8869–8880.

Deacon, G. E. R., 1977: Comments on a counterclockwise circulation in the Pacific subantarctic sector of the Southern Ocean suggested by McGinnis. *Deep-Sea Res.*, **24,** 927–930.

deSzoeke, R. A., 1987: On the wind-driven circulation of the South Pacific Ocean. *J. Phys. Oceanogr.*, **17,** 613–630.

Effron, B., 1979: Computers and the theory of statistics: Thinking the unthinkable. *SIAM Rev.*, **21,** 460–480.

Fu, L.-L., and D. B. Chelton, 1985: Observing large-scale temporal variability of ocean currents by satellite altimetry: With application to the Antarctic Circumpolar Current. *J. Geophys. Res.*, **90,** 4721–4739.

Gill, A. E., 1968: A linear model of the Antarctic circumpolar current. *J. Fluid Mech.*, **32,** 465–488.

——, and P. P. Niiler, 1973: The theory of seasonal variability in the ocean. *Deep-Sea Res.*, **20,** 141–177.

Godfrey, J. S., 1989: A Sverdrup model of the depth-integrated flow for the world ocean allowing for island circulation. *Geophys. Astrophys. Fluid Dyn.*, **45,** 89–112.

Gordon, A. L., E. Molinelli, and T. Baker, 1978: Large-scale relative dynamic topography of the Southern Ocean. *J. Geophys. Res.*, **83,** 3023-3032.

Greatbatch, R. J., and A. Goulding, 1989: Seasonal variations in a linear barotropic model of the North Pacific driven by the Hellerman and Rosenstein wind stress field. *J. Geophys. Res.*, **94,** 12 645–12 665.

Inoue, M., 1985: Modal Decomposition of the low-frequency currents and baroclinic instability at Drake Passage. *J. Phys. Oceanogr.*, **15,** 1 158–1 181.

Johnson, G. C., and H. L. Bryden, 1989: On the size of the Antarctic Circumpolar Current. *Deep-Sea Res.*, **36,** 39–53.

Koblinsky, C. J., 1990: The global distribution of f/H and the barotropic response of the ocean. *J. Geophys. Res.*, **95,** 3213–3218.

——, P. P. Niiler, and W. J. Schmitz, Jr., 1989: Observations of wind-forced deep ocean currents in the North Pacific. *J. Geophys. Res.*, **94,** 10 773–10 790.

Large, W. G., and S. Pond, 1982: Sensible and latent heat flux measurements over the ocean. *J. Phys. Oceanogr.*, **12,** 464–482.

——, and H. van Loon, 1989: Large-scale, low-frequency variability of the 1979 FGGE surface buoy drifts and winds over the Southern Hemisphere. *J. Phys. Oceanogr.*, **19,** 216–232.

Mulhearn, P. J., 1987: The Tasman Front: A study using satellite infrared imagery. *J. Phys. Oceanogr.*, **17,** 1148–1155.

Neumann, G., 1955: On the dynamics of wind-driven ocean currents. *Meteor. Papers*, **2,** 33 pp.

Peterson, R. G., 1988: On the transport of the Antarctic Circumpolar Current through Drake Passage and its relation to wind. *J. Geophys. Res.*, **93,** 13 993–14 004.

Reid, J. L., 1986: On the total geostrophic circulation of the South Pacific Ocean: Flow patterns, tracers and transports. *Progress in Oceanography*, Vol. 16, Pergamon, 1–61.

Stanton, B. R., 1981: An oceanographic survey of the Tasman Front. *N.Z. J. Mar. Freshwater Res.*, **15,** 289–297.

Stommel, H., 1957: A survey of ocean current theory. *Deep-Sea Res.*, **4,** 149–184.

Sverdrup, H. U., 1947: Wind-driven currents in a baroclinic ocean: With application to the equatorial currents in the eastern Pacific. *Proc. Natl. Acad. Sci. U.S.A.*, **33,** 318–326.

Trenberth, K. E., W. G. Large, and J. G. Olson, 1990: The mean annual cycle in global ocean wind stress. *J. Phys. Oceanogr.*, **20,** 1742–1760.

Whitworth, T., and R. G. Peterson, 1985: The volume transport of the Antarctic Circumpolar Current from bottom pressure measurements. *J. Phys. Oceanogr.*, **15,** 810–816.

Willebrand, J., S. G. Philander, and R. C. Pacanowski, 1980: The oceanic response to large-scale atmospheric disturbances. *J. Phys. Oceanogr.*, **10,** 411-429.

Wyrtki, K., 1971: *Oceanographic Atlas of the Indian Ocean Expedition.* National Science Foundation NSF-10E-1, 531 pp.